J. Ind. Geophys. Union (November 2018)
v.22, no.6, pp: 585-597

Comparing pre- and post- stack seismic inversion methods - a case study from Scotian Shelf, Canada

S.P. Maurya* and N.P. Singh

[1]Department of Geophysics, Institute of Science, Banaras Hindu University Varanasi-221005, U.P., India
*Corresponding author: spm.bhu@gmail.com

ABSTRACT

In the present study, pre- and post-stack seismic inversions are performed to estimate subsurface petrophysical properties from the seismic reflection data, obtained over the Penobscot field, Canada. Such methods are routinely used to estimate subsurface property from seismic reflection data but the problem arises in deciding which method will provide more efficient and detailed information of the subsurface structures. Simple procedure is used here at the every step of seismic inversion methods, differences have been taken between pre- and post- stack seismic inversion. It is broadly applied in two steps; first, they are applied to the composite trace near to well location and inverted to obtain petrophysical parameters, which are then compared with the well log data. The analysis shows that both curves (inverted and well log) are in good agreement and display high correlation. The average correlation of post stack inversion (0.92), is higher than the pre-stack seismic inversion method (0.89). In the second step, entire seismic section is inverted and P- impedance, S- impedance, density, P- wave velocity, S- wave velocity and V_P/V_S ratio are estimated. The post stack inversion methods provide only acoustic impedance which is transformed into the other petrophysical parameters, using relationship derived from the well log data. These parameters are helpful in interpreting seismic sections. The analysis shows that both (pre- and post- stack) methods produces subsurface property in similar way, with high resolution from post-stack inversion, compared to the pre-stack inversion. Although the pre-stack inversion method produces more petrophysical parameters that are sensitive towards fluid and rock property, but the resolution is relatively poorer compared to the post-stack inversion methods. The interpreted inverted section indicates that the studied area does not have any major hydrocarbon accumulation.

Keywords: Pre- and Post- stack seismic inversion, Well log analysis, Amplitude spectrum, Petrophysical properties, Scotian shelf Canada

INTRODUCTION

Seismic inversion is a technique that estimates subsurface petrophysical properties from seismic reflection data with the integration of well log data. These petrophysical parameters help to interpret acquired seismic section (Krebs et al., 2009). In hydrocarbon industry, seismic inversion techniques are used as a tool to locate hydrocarbon-bearing strata at subsurface depths (Morozov and Ma, 2009; Lindseth, 1979).The physical parameters that are of interest to a modeler performing inversions are impedance (Z), P-wave (V_P) and S-wave (V_S) velocity, apart from density. Lame parameters that are more sensitive towards fluid and saturation in rocks (Clochard et al., 2009) can also be derived from inverted impedance. Similarly, the other petrophysical parameters like porosity, sand/shale ratio and gas saturation too can be estimated with the help of inverted volumes (Goodway, 2001). A reliable estimate of the reservoir properties is critical in decision-making process, especially during developmental phase (Pendrel, 2006).

Basically, the seismic inversion techniques can be divided into two broad categories, post-stack and pre-stack inversion. The first approach is the most commonly used, where the effect of the wavelet is removed from the seismic data and high-resolution images of the subsurface are produced (Chen and Sidney, 1997). The second approach relies mainly on model building from well log, seismic and geological data (Downton, 2005). This method also generates high-resolution images of the subsurface

The advantages of post-stack inversion are many. For example, (i) stratigraphic interpretation is easier on impedance data than seismic data, (ii) the reduction of wavelet effects, side lobes and tuning enhances the resolution of subsurface layers, (iii) the acoustic impedance can be directly computed and compared to well log measurements, that serve as a link to reservoir properties, (iv) porosity can be related to the acoustic impedance using geostatistical methods, these impedance volumes can be transformed into the porosity volumes, (v) The acoustic impedance can be utilized to locate individual reservoir regions, (vi) it takes very less time than pre-stack inversion, and (vii) it does not give shear wave information to discriminate the fluid effects (Russell, 1999; Morozov and Ma, 2009; Maurya and Singh, 2015; Maurya et al., 2018a).

Similarly, the elastic properties of the subsurface such as S- wave velocity of the subsurface layers, which are sensitive to the fluid saturation can be obtained from

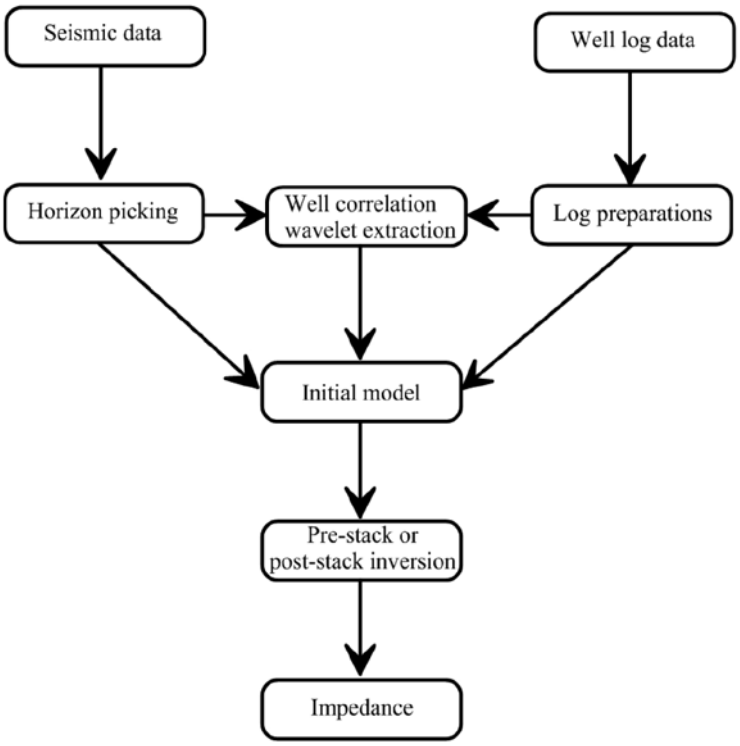

Figure 1. Flowchart of seismic inversion methods.

pre-stack inversion (Moncayo et al., 2012). This method transforms seismic reflection data into P- impedance, S-impedance, density and Vp/Vs ratio sections, through the integration of well log data and horizon information from seismic reflection data. P- impedance and V_P/V_S ratio are considered reliable, depending on the target depth and acquisition configuration, and thus can be used to predict reservoir properties away from well locations (Carrazzone et al., 1996). Pre-stack seismic inversion also provides several benefits that include (i) P- impedance, S- impedance and density which is layer property, whereas seismic data is an interface property, (ii) enhancement of the resolution of sub-surface layers due to reduction of wavelet effects, tuning and side lobes, (iii) acoustic impedance can be directly compared to well log measurements, which in turn are linked to the reservoir properties, and (iv) compared with other inversion techniques (e.g. post-stack inversion), the data offers additional information to distinguish between lithology and fluid effects (Gholami, 2016).

Further, wavelet is very crucial part of seismic inversion methods. During seismic inversion, one integrates seismic and well log data together, but both are in different domain (one is in time and other is in depth) and hence needed to convert in same domain. For that reason, wavelet is extracted from the seismic section and the process used includes (i) extraction of the analysis window in seismic section, (ii) applying Taper at the start and end of the seismic window, (iii) calculate the autocorrelation of the data window, (iv) calculate the amplitude spectrum of the autocorrelation, (v) calculate the square root of the autocorrelation spectrum. This process approximates the amplitude spectrum of the wavelet, (vi) add phase of the wavelet, and then finally, the inverse Fast Fourier Transform gives the desired wavelet (Vardy et al., 2018, Maurya et al., 2018b).

In the present study, comparison of pre- and post-stack seismic inversion methods have been performed and their relative performance is estimated in each intermediate steps. For the analysis, pre-stack gather from the Penobscot region, is used along with one well (L-30). The inversion is first tested for composite trace near to well location and then performed to the entire gathers. A variety of attributes i.e. P- impedance, S- impedance, P- wave, S- wave velocity, density and V_P/V_S ratio is estimated in inter-well region from pre-stack inversion methods, while only P- impedance is estimated from the post-stack inversion methods. Thereafter, the P-impedance from the post-stack inversion method is transformed into S- impedance, P- wave, S- wave velocity, density and V_P/V_S ratio, using relationship derived from well log data. Thereafter, point by point comparison is performed between attributes derived from pre- and post-stack seismic inversion methods. The inversion is performed using Hampson Russell software (10.2) and the analysis of the inversion results are carried out using Matlab programming language (Matlab, 2015b). Figure 1 shows flowchart of seismic inversion methods used in this study.

Figure 2. Map showing Penobscot study area highlighted by red rectangle.

STUDY AREA

The present study area Penobscot lies in the Scotian shelf (Figure 2) in offshore Nova Scotia, Canada. The survey contains several structural and stratigraphic features. Two major faults within the survey area that form an echelon pattern (Campbell et al., 2015), can be seen in the seismic sections. This fault mostly displaces the interpreted surfaces horizons. The seismic attributes, particularly multi-trace similarity, volumetric curvature or volumetric amplitude highlight these features more clearly (Cummings and Arnott, 2005). The measured seismic signal is poor below 3.0 seconds in length (about 5km). Two wells, L-30 and B-41, were drilled in the area penetrating Misaine and Baccaro members of the Jurassic Abenaki Formation (Kidston et al., 2005). The data used in this study contains inline 1161-1200 and cross-line 1000-1481 with one well (L-30). Several oil and gas fields are located in this Late Jurassic to Cretaceous intervals. The Lower Logan Canyon sands in L-30 were considered oil bearing (minor accumulation) (Smith and Gidlow 1987).

The seismic and well data have been downloaded from the OpendTect seismic data portal. The time to depth models have been taken from the CNSOPB report (Kidston et al., 2005). The survey contains a limited range of pre-stack data. The data covers many geological features, which include graben-bounded faults, channels, mega-scale de-watering faults and reefs (Kidston et al., 2007).

METHODOLOGY

Pre-stack inversion

The pre-stack inversion technique utilizes pre-stack CMP gather to estimate P- impedance (Z_P), S- impedance (Z_S), density (ρ) and V_P/V_S ratio. The P- and S- impedance are related to each other in wet clastic rocks and also according to Castagna equation (Eq. 1), the P- wave velocity is related to the S- wave velocity (Castagna et al., 1985) in following way.

$$V_p = 1.16V_s + 1360 \quad (1)$$

Further, according to the Gardner equation (Eq. 2), the P-wave velocity is related to the density (Gardner et al. 1974) as

$$\rho = 0.23V^{0.25} \quad (2)$$

Therefore, pre-stack seismic inversion uses these relationships to derive following equations.

$$\ln(Z_S) = k\ln(Z_P) + k_C + \Delta L_S \quad (3)$$

$$\ln(\rho) = m\ln(Z_P) + m_C + \Delta L_D \quad (4)$$

where coefficients (k, k_c, m *and* m_c) are calculated using well log cross plot and ΔL_S and ΔL_D represent the deviation from

the best fitted line. The Aki-Richard's equation is redefined by Fatti as followings (Fatti et al., 1994).

$$R(\theta) = c_1 \frac{\Delta V_P}{V_P} + c_2 \frac{\Delta V_S}{V_S} + c_3 \frac{\Delta \rho}{\rho} \quad (5)$$

where $c_1 = \frac{1}{2cos^2\theta}$, $c_2 = 0.5 - \left(\frac{V_S}{V_P}\right)^2 sin^2\theta$ and $c_3 = 4\left(\frac{V_S}{V_P}\right)^2 sin^2\theta$

The above equation estimate reflection coefficient as a function of incident angle θ. For a given angle T (θ), we can therefore derive a relationships between the *P*- impedance, *S*-impedance and density by modifying Fatti's equation (Fatti et al. 1994) to obtain following equation:

$$T(\theta) = C_1 W(\theta) * DL_P + C_2 W(\theta) * DL_S + C_3 W(\theta) * DL_D \quad (6)$$

Where $L_P = \ln(Z_P)$, $L_S = \ln(Z_S)$, and $L_D = \ln(\rho)$. The other constants values are like $c_1 = \frac{1}{2}c_1 + \frac{1}{2}Kc_2 + mc_3$, $C_2 = \frac{1}{2}c_2$, $W(\theta)$ is the wavelet at angle θ, D is the differentiation derivative operator. If in the above equation θ=0 then this equation reduces to zero-offset (model-based) inversion methods (Shu-jin, 2007). The equation (6) can be implemented in matrix form as following.

$$\begin{bmatrix} T(\theta_1) \\ \vdots \\ T(\theta_N) \end{bmatrix} = \begin{bmatrix} C_1(\theta_1)W(\theta_1)D & \cdots & C_3(\theta_3)W(\theta_3)D \\ \vdots & \ddots & \vdots \\ C_1(\theta_N)W(\theta_N)D & \cdots & C_3(\theta_N)W(\theta_N)D \end{bmatrix} \quad (7)$$

Solve the above matrix by matrix inversion methods, and initialize the solution to $[L_P \Delta L_S \Delta L_D] = [ln(Z_{P0}\ 0\ 0)]$, where Z_{P0} is the initial impedance model.

Post-stack inversion

There are many types of post stack seismic inversion algorithm available but in the present study, Model based inversion (MBI) algorithm is used for the analysis. MBI is based on the convolution theory, which states that the seismic trace can be generated from the convolution of wavelet with the earth`s reflectivity and addition of noise (Mallick, 1995),

$$S(t) = W(t) * r(t) + n(t) \quad (8)$$

Where *S(t)*, *W(t)*, *r(t)* and *n(t)* are synthetic trace, wavelet, earth reflectivity and noise component respectively. If the noise in the data is uncorrelated with the seismic signal, the trace can be solved for the earth reflectivity function. This is a non-linear equation which can be solved iteratively as follows (Latimer et al., 2000):

$$Z = V\rho \quad (9)$$

$$r_i = \frac{Z_{i+1} - Z_i}{Z_{i+1} + Z_i} \quad (10)$$

$$Z_N = Z_1 exp\left(\sum_{i=1}^{N} r_i\right) \quad (11)$$

These equations are used in practice for recursive inversion with the aim of transforming reflectivity function into acoustic impedance (Berteussen and Ursin, 1983). Z_1 is the acoustic impedance of first (top) layer and Z_N is the AI of Nth layer, r_i is the reflection coefficient at ith interface. This equation is valid for most of the practical cases where $r_j \leq |0.3|$ (Berteussen and Ursin, 1983).

The acoustic impedance model of low frequency is obtained by estimating these values over the entire seismic section using kriging interpolation techniques at the wells (Maurya and Singh 2017; Schuster, 2017). Generally, acoustic impedance is not recorded during the acquisition of well log data. These parameters can be estimated directly from the sonic and density log. The objective function which needs to minimize is:

$$e(r) = \alpha \sum_{j=1}^{M} |r_j| + \frac{1}{2} \| \frac{1}{\sigma}(S - W * r) \|^2 \quad (12)$$

The least squares optimization is performed for minimizing the difference between the real and the modeled reflectivity section. This is achieved by analyzing the misfit between the synthetic trace and the real trace and modifying the block size and the amplitude to reduce the error (Ferguson and Margrave, 1996).

LMR Transform

The LMR (Lambda-mu-rho) method was originally proposed by Goodway et al., (1997). LMR uses the following relationships between V_P, V_S, ρ and the Lame parameters - Lambda (λ) and Mu (μ):

$$V_P = \sqrt{\frac{\lambda + 2\mu}{\rho}} \quad (13)$$

and

$$V_S = \sqrt{\frac{\mu}{\rho}} \quad (14)$$

Therefore,

$$Z_S^2 = (\rho V_S)^2 = \mu\rho \quad (15)$$

and

$$\lambda\rho = Z_P^2 - 2Z_S^2 \quad (16)$$

Through seismic inversion, the above equations express P-impedance and S-impedance in rock properties. It is claimed that λρ and μρ help to discriminate fluid effects from lithology effects (Srivastava and Maultzsch 2018).

RESULTS AND DISCUSSIONS

Before moving towards seismic inversion methods, the seismic reflection data needs to be pre-conditioned to increase the signal to noise ratio. There are five major steps that are used to improve seismic signal i.e. Bandpass filtering, Muting, Super gather, Parabolic radon transform and Trim statics. Figure 3 displays output of pre-conditioning, where Figure 3a shows raw seismic gather at inline 1161, Figure 3b

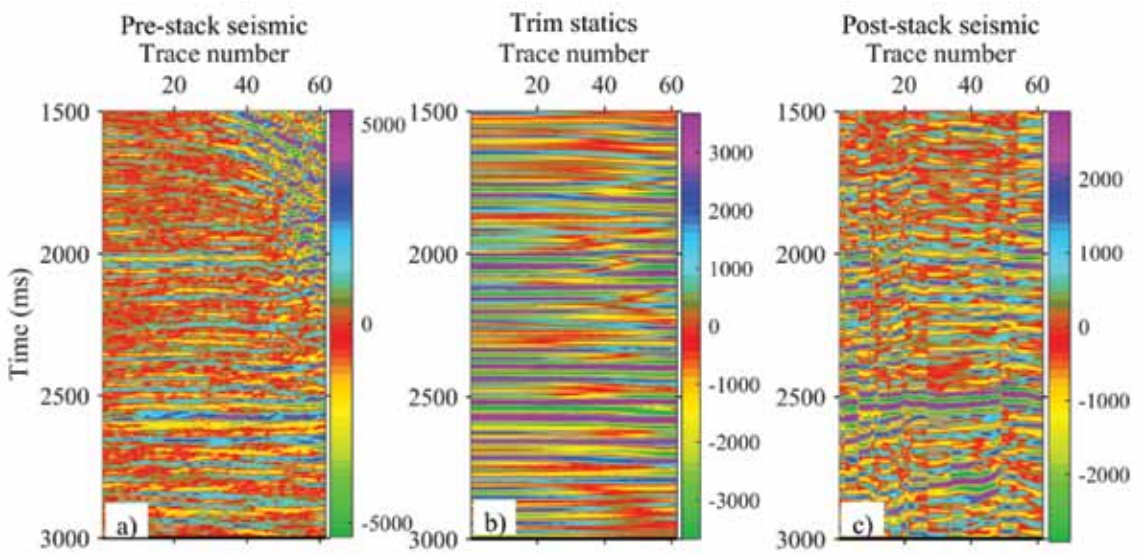

Figure 3. a) Penobscot pre-stack seismic gather, b) Trim statics gather and c) CDP stack section.

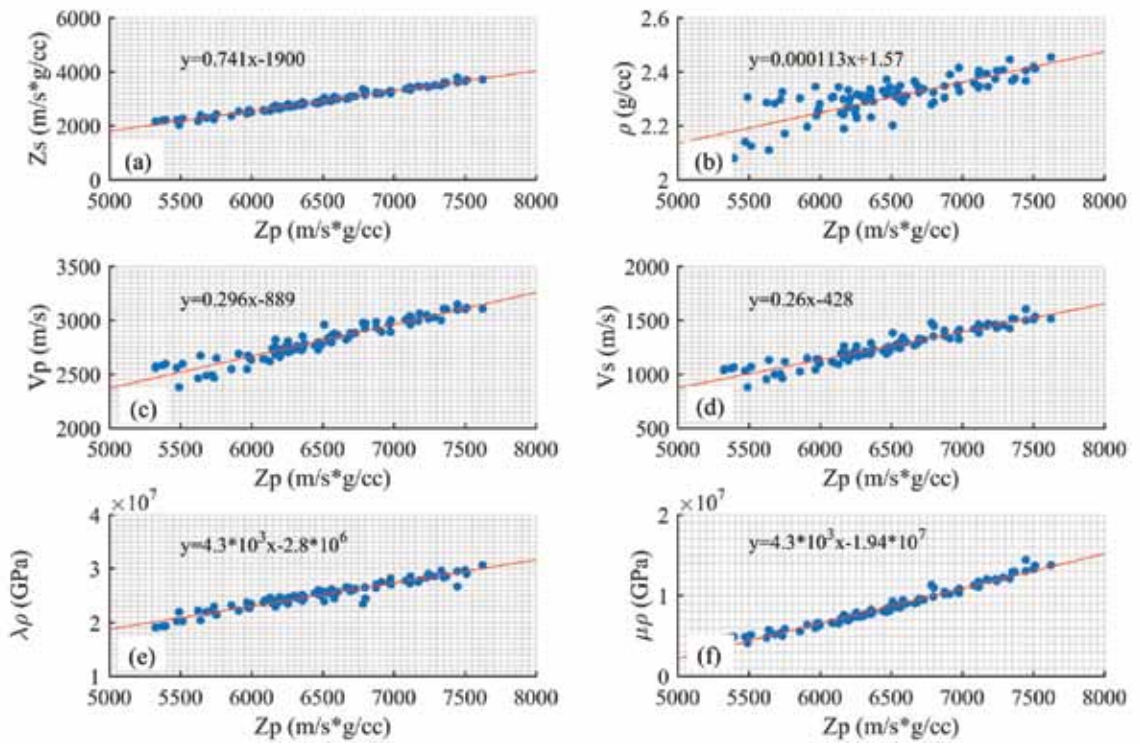

Figure 4. Well log crossplots. (a) Z_P versus Z_S, (b) Z_P versus density, (c) V_P versus Z_P, (d) V_S versus Z_P, (e) λρ versus Z_P and (f) μρ versus Z_P.

illustrate trim static gather generated after pre-conditioning, and Figure 3c shows stack section. Pre-stack trim static gather is used by pre-stack inversion methods, whereas stack section is used by post-stack seismic inversion methods.

Seismic pre-stack inversion methods estimate P-impedance (Z_P), S- impedance (Z_S), Density (ρ), V_P/V_S ratio, lambdarho (λρ) and murho (μρ), whereas post-stack inversion methods estimate P- impedance only. To compare other petrophysical parameters, the post-stack impedance is transformed into S- impedance, density, V_P/V_S ratio, lambdarho (λρ) and murho (μρ) sections, using relationship derived from well log data. Figure 4 depicts crossplot of well log curves to derive relationship between them. Figure 4a shows crossplot of Z_P versus Z_S, figure 4b depicts crossplot of Z_P versus density, and Figures 4c-f depict crossplots of V_P, V_S, λρ and μρ with respect to Z_P respectively.

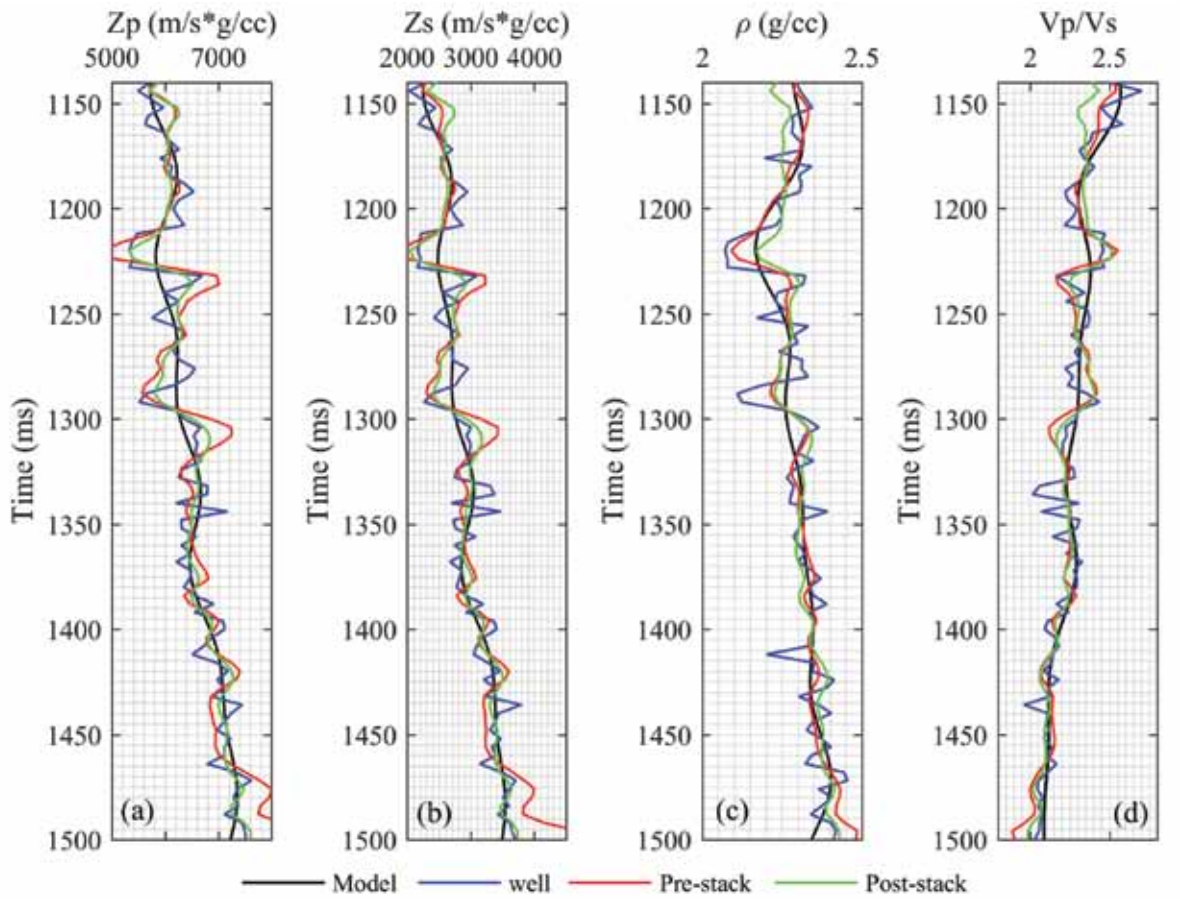

Figure 5. Seismic inversion analysis plot for well L-30 where (a) shows comparison of P-impedance, (b) S-impedance, (c) density, and (d) V_P/V_S ratio.

A best fit straight line gives the relationship among petrophysical parameters, as given below

$$Z_S = 0.741Z_P - 1900 \quad (13)$$

$$\rho = 0.000113Z_P + 1.57 \quad (14)$$

$$V_P = 0.296Z_P + 889 \quad (15)$$

$$V_S = 0.26Z_P - 428 \quad (16)$$

$$\lambda\rho = 4.3 \times 10^3 Z_P - 2.8 \times 10^6 \quad (17)$$

$$\mu\rho = -0.00023Z_P + 3.76 \quad (18)$$

Using these relationships (Eq. 13-18), inverted P-impedance from the post stack inversion is transformed into the S- impedance, density, V_P/V_S ratio, lambdarho ($\lambda\rho$) and murho ($\mu\rho$) sections.

The inversion methods has been applied in two steps, firstly, one composite trace near to well location (L-30, inline 1177, xline 1153) is extracted and inverted for petrophysical parameters to cross verify the results. Figure 5 depicts comparison of inverted results with well log. Figure 5a shows comparison of P-impedance, Figures 5b, 5c and 5d show comparison of S-impedance, density and V_P/V_S from inverted results and well log curves. From Figure 5, it is noticed that the inverted curves from pre- and post- stack inversion methods agree well with the well log curves. The only difference noticed here is that the post-stack curves are more close to the well log compared with the pre-stack results. The error analysis among all the inverted parameters are performed and described in table 1.

Figure 6 depicts crossplot of inverted petrophysical parameters with the well log petrophysical parameters for the Quality check (QC) of the inverted results. Figure 6a depicts crossplot of inverted and original (well log) P-impedance, while Figures 6b, 6c and 6d depict crossplot of inverted and original S- impedance, density and V_P/V_S ratio respectively. In Figure 6, the blue circle indicates inversion results from pre-stack inversion methods while the red circle indicates post-stack inversion results. The distribution of scatter points from the best fit line indicates that the inverted results are very close to the original values as the point's lies very close to the best fit line for both the cases.

After getting satisfactory results from the composite trace, both inversion methods (pre- and post- stack) are applied to the seismic volume to estimate rock properties of the subsurface. Figure 7 depicts cross-section of inverted P- impedance for inline 1161. Figure 7a shows impedance cross-section generated using pre-stack inversion algorithm, Figure 7b depicts cross-section of impedance generated

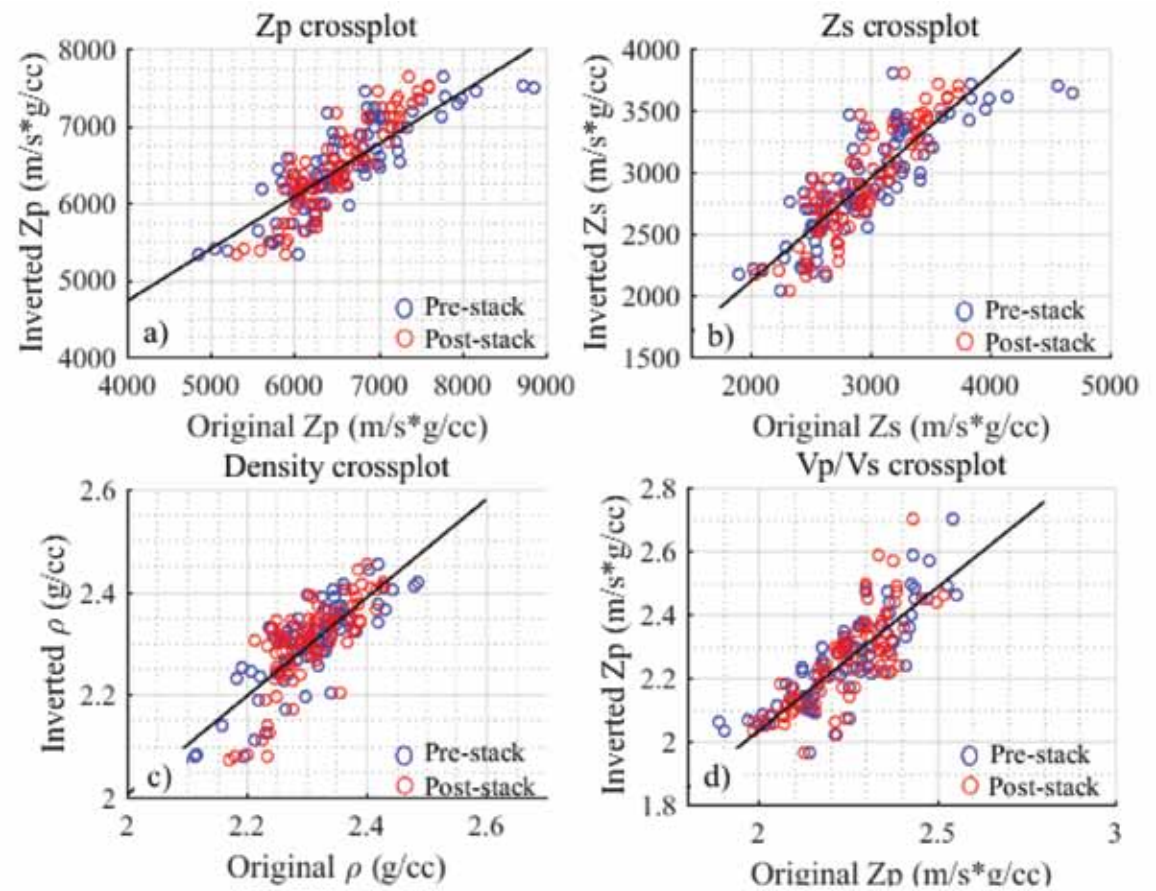

Figure 6. Crossplot of inverted and original, (a) P-impedance, (b) S-impedance, (c) density, and (d) V_P/V_S ratio.

using post-stack seismic inversion method and Figure 7c depicts difference between pre- and post-stack impedance sections. From Figure 7, it can be noticed that both the inversion methods (pre- and post-stack) give similar type of results with least differences between them. The relatively large differences (300-800 m/s*g/cc) are observed at later time which may be due to presence of high impedance contrast in this zone.

Figure 8 shows cross-section of inverted S- impedance at inline 1161. Figure 8a depicts cross-section of S-impedance generated using pre-stack inversion technique, Figure 8b shows cross-section of S-impedance generated using post-stack inversion and Figure 8c shows difference between them. From Figure 8, it is noticed that both the inversion methods give high resolution images of the subsurface in similar way with least differences between them. The relatively large differences (200-500 m/s*g/cc) are observed because of S- impedance is inverted from pre-stack inversion directly, whereas the S-impedance is derived from post-stack P-impedance using well log relation which holds good hold for trace near to well location and shows small deviation far traces away from the borehole.

Figure 9 shows cross-section of inverted density at inline 1161 only for simplicity. Figure 9a depicts cross-section of density generated using pre-stack inversion algorithm, Figure 9b depicts cross-section of density generated using post-stack seismic inversion method and Figure 9c shows density differences between pre - and post-stack inverted results. It is noticed from Figure 9 that both the inversion methods again give similar type of results of the subsurface, with very small differences between them. The relatively large differences (0.1-0.3 g/cc) are observed in middle time interval that may be due to transformation of P- impedance into density section from post-stack inversion while pre-stack inversion methods estimate density sections directly although the differences are negligible.

Figure 10 shows cross-section of inverted λρ at inline 1161, wherein Figure (a) shows inverted λρ generated using pre-stack inversion, while Figure (b) to that generated using post-stack seismic inversion utilizing relationship from well log data. Similarly, Figure (c) reveals the differences between pre-stack and post-stack generated λρ section. It can be noticed from these figures that both the inversion methods (pre- and post-stack) give similar type of results with very small differences between them. The relatively large differences (1-5GPa*g/cc) are observed in middle time interval that may be due to the transformation of P-impedance into λρ section from post-stack inversion

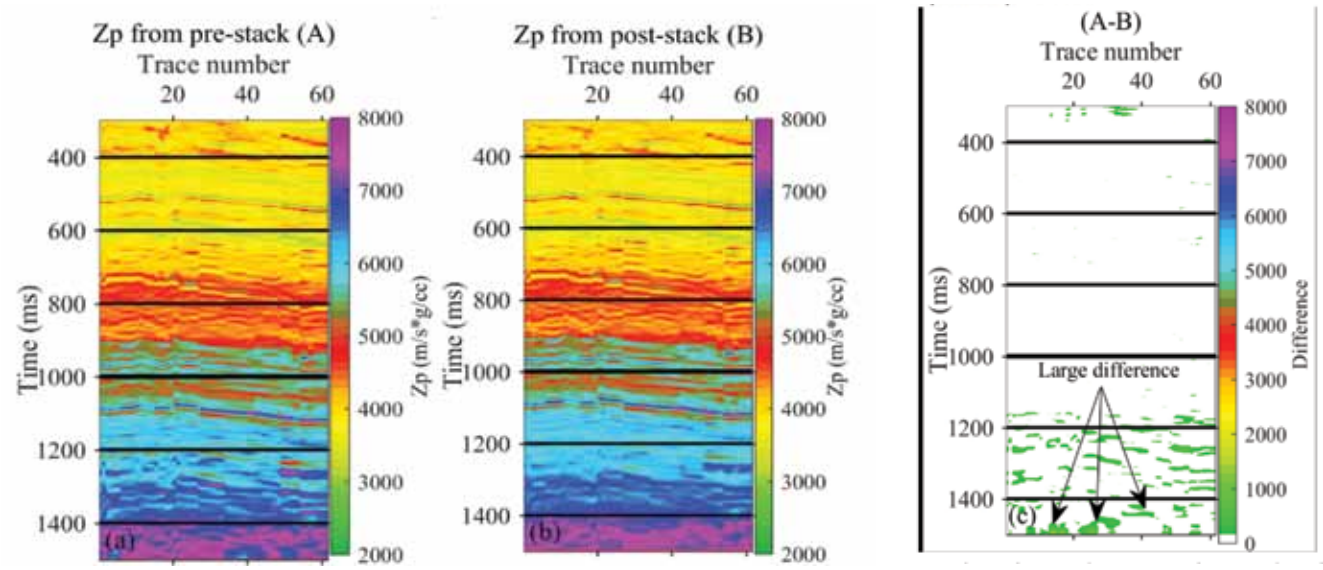

Figure 7. Cross-section of inverted P- impedance estimated using (a) pre-stack, (b) post-stack inversion, and (c) difference between them.

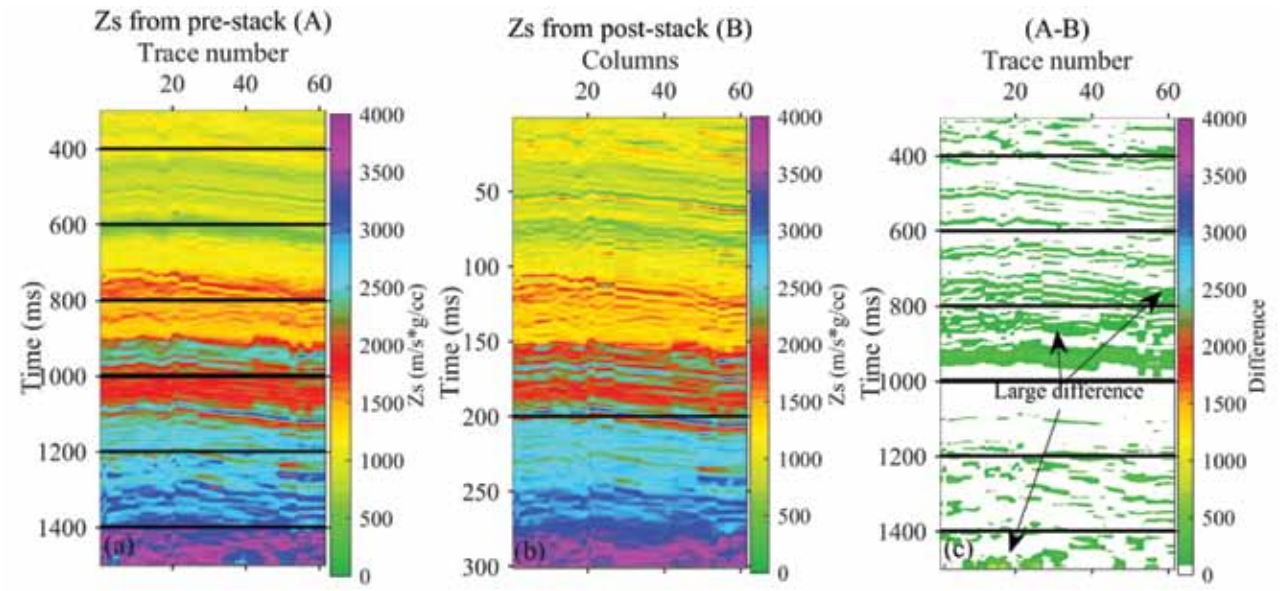

Figure 8. Cross-section of inverted S-impedance estimated using a) pre-stack, b) post-stack inversion and (c) difference between them.

while pre-stack inversion methods estimate λρ sections directly.

Figure 11 shows cross-section of inverted μρ at inline 1161 for simplicity, although the inversion is performed for entire volume (inline 1161-1200, cross-line 1000-1481). Figure (a) shows cross-section of μρ generated using pre-stack inversion algorithm while Figure (b) depicts cross-section of μρ generated using post-stack seismic impedance inversion using well log relation. Similarly, Figure (c) shows differences of μρ between pre- and post-stack results. Similar types of results are found from both the inversion methods with very small difference between them. The relatively large differences (1-5 GPa*g/cc) are observed in the middle time interval.

Table 1 illustrates quantitative differences between pre- and post-stack inverted results. Column 1 of table 1 depicts parameters to be compared, column 2 and 3 depict correlation and RMS error for pre-stack inversion, while column 4 and column 5 illustrates correlation and RMS error for post-stack seismic inversion methods. The quantitative values show that the inverted results from the post stack inversion are more efficient and close to

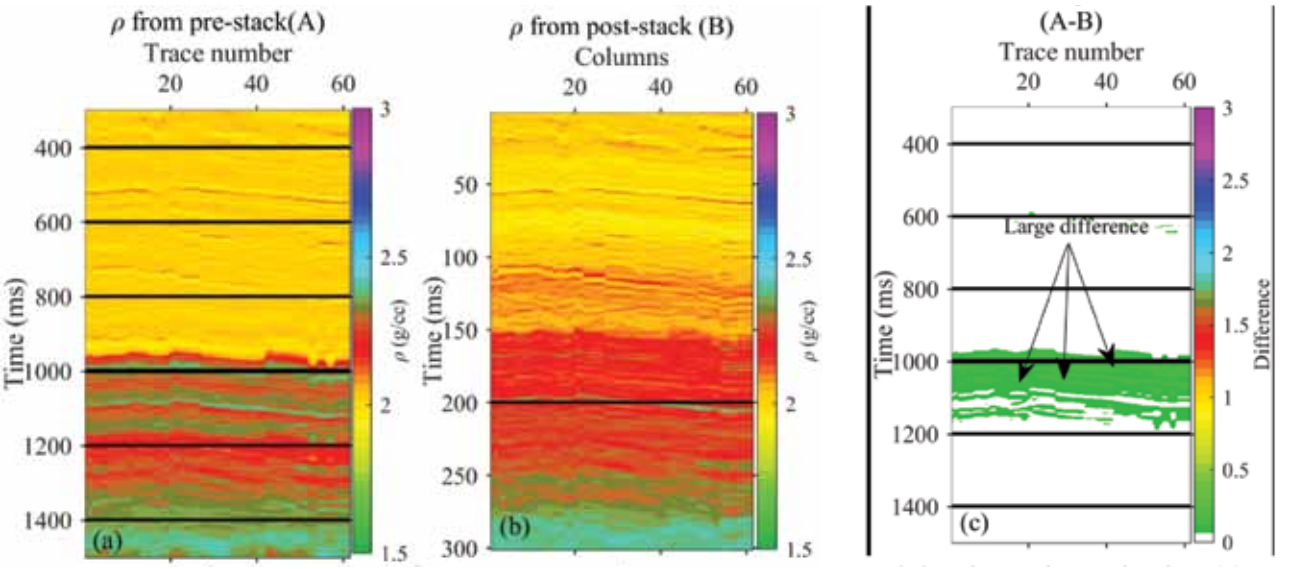

Figure 9. Cross-section of inverted density estimated using (a) pre-stack, (b) post-stack inversion and (c) difference between them.

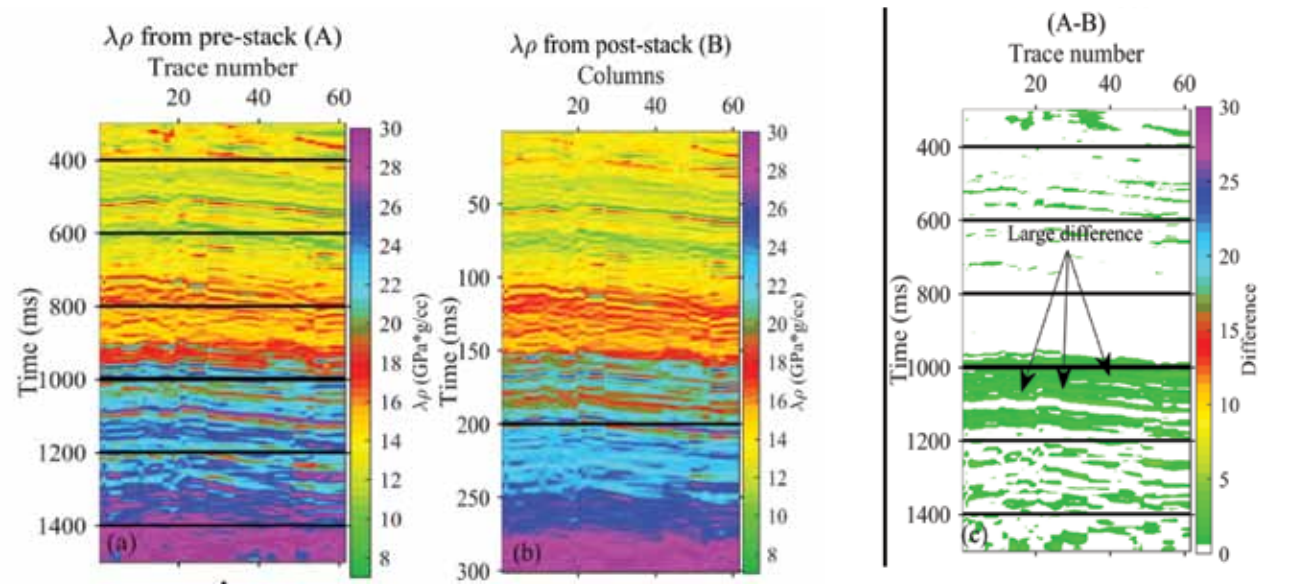

Figure 10. Cross-section of inverted λρ estimated using (a) pre-stack and (b) post-stack inversion. Figure (c) shows the difference between the two.

the original results compared to the pre-stack inversion methods. The interpretation of inverted section shows continuous variation of murho parameters in the subsurface and it indicates non-availability of reservoir.

Further, the porosity is predicted in inter-well region by using acoustic impedance generated from pre- and post- stack seismic inversion methods. Generally, this property is predicted using neural network, or single attribute regression or multi attribute regression etc. but these tools required more than one well in the area, hence cannot be used in the present study as the area does have only one well (L-30). An alternative way has been used in the present study to estimate porosity section from the impedance section, i.e. to use relationship between porosity and impedance derived from the well log data. This type of relationship holds good for traces near to well location, but shows small deviation and quantitative interpretation cannot be performed accurately. Initially, well log porosity and impedance is cross plotted (Figure 12) and a best fit straight line give relationship between these two quantities. The estimated relation between density porosity (φ) and impedance (Z_P) can be given as

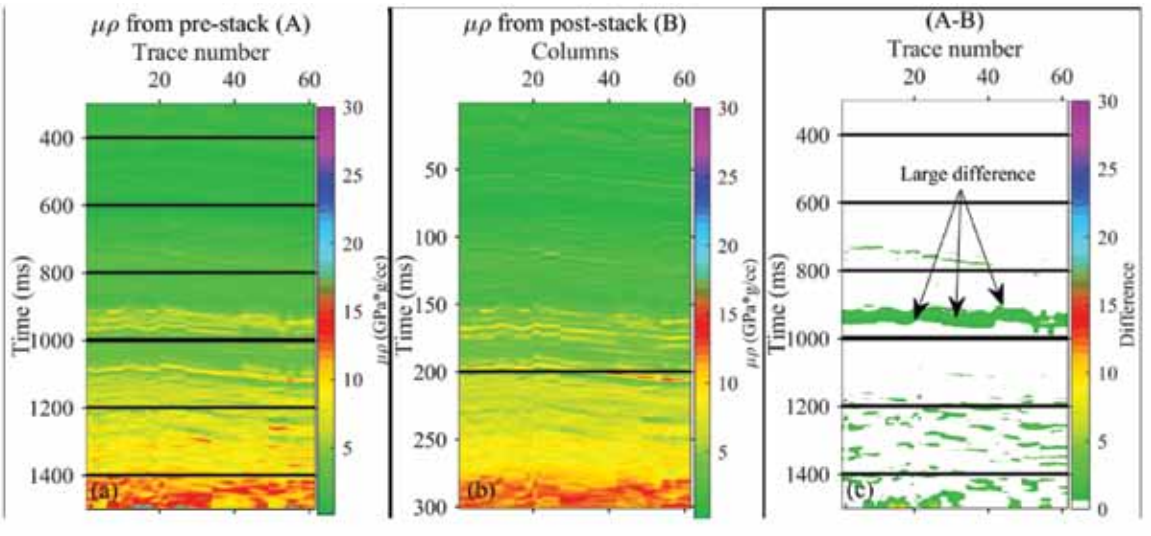

Figure 11. Cross-section of inverted $\mu\rho$ estimated using (a) pre-stack, (b) post-stack inversion, and (c) difference between the two.

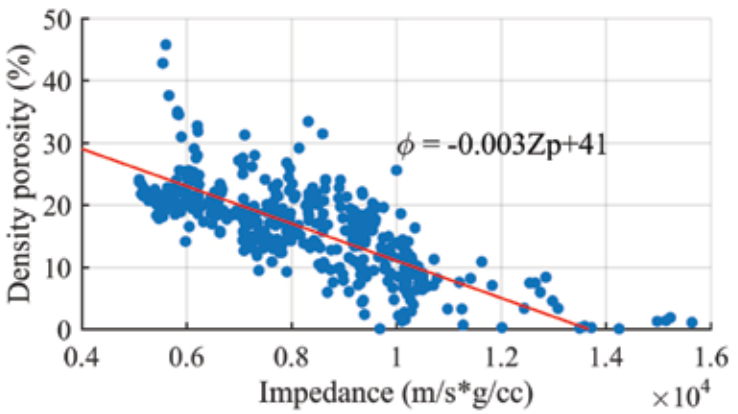

Figure 12. Crossplot of well log porosity and well log impedance.

Table 1. Comparison of inversion results.

S.No.	Parameters	Pre-stack		Post-stack	
		Correlation	RMS Error	Correlation	RMS Error
1.	P-impedance	0.99	0.06	0.94	0.11
2.	S-impedance	0.92	0.15	0.89	0.18
3.	Density	0.93	0.13	0.90	0.16
4.	Vp/Vs	0.89	0.22	0.88	0.30
5.	λρ	0.91	0.19	0.87	0.32
6.	μρ	0.90	0.18	0.88	0.29

$$\phi = -0.003Z_P + 41 \quad (19)$$

Using equation 19, acoustic impedances estimated from pre- and post - stack inversion methods are transformed into porosity section. Figure 13 depicts cross-section of estimated porosity from acoustic impedance. Figure (a) shows porosity section generated from pre-stack seismic inverted impedance, while Figure (b) shows porosity section generated from post-stack inverted impedance. Similarly, Figure (c) shows difference between them. As the impedance and porosity is closely related to each other, hence the cross-section of porosity shows very high resolution of subsurface porosity. The Figures demonstrate that almost

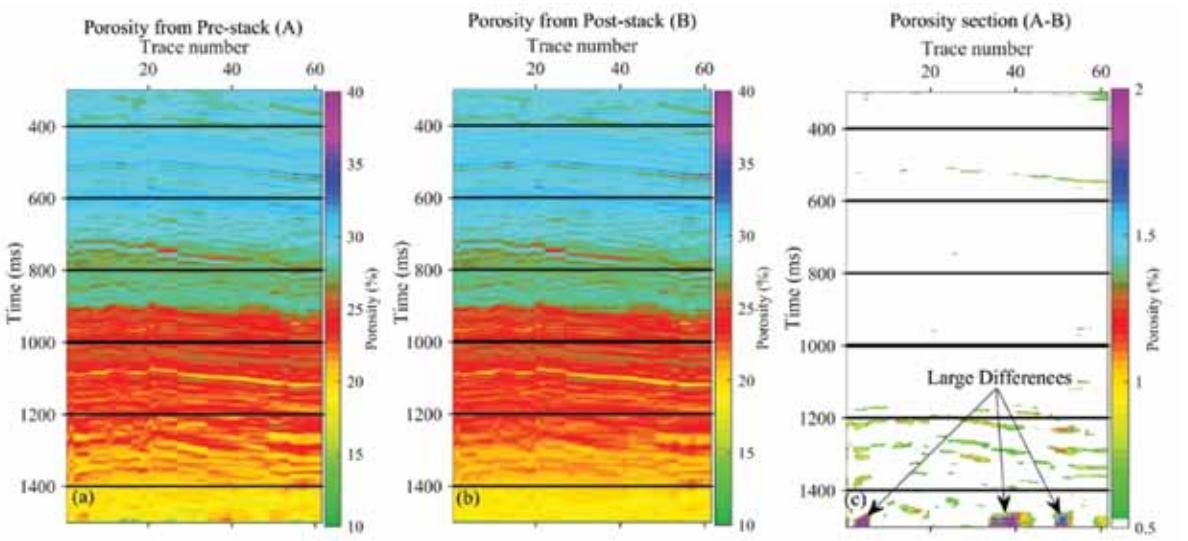

Figure 13. Cross-section of inverted $\mu\rho$ estimated using (a) pre-stack, (b) post-stack inversion and (c) difference between them.

both methods estimate porosity in similar way with only 3 very small patches of large difference seen which is highlighted in the Figure 13c. The porosity section shows continuous variation of porosity and does not indicate any high porosity patches and confirm non-existence of any major reservoir in this zone.

From the analysis it is concluded that the pre - and post - stack inversion methods provides similar results with higher resolution from post-stack methods, however this method only estimate P-impedance. On the other hand pre-stack inversion methods estimate variety of attributes i.e. P- impedance, S- impedance, density, V_P/V_S ratio, lambdarho and murho. Relationships are derived from well log data and used to transform P- impedance from post stack into attributes and compared with pre-stack. It is noticed that the derived Z_S, Density, V_P/V_S ratio, lambdarho and murho are following trend from well log data nicely. The difference among these petrophysical parameters demonstrate that both methods produces similar results, with small deviation, particularly where larger values are present. These differences also arise due to use of equations from well log data which is best suited for the traces which are very close to the well log data and shows deviation away from the boreholes. The interpretation of inverted results indicates non-existence of any major reservoir. Due to presence of reservoir, low impedance and corresponding high porosity patches should appear but in the present study continuous variation of derived parameters have been noticed.

CONCLUSIONS

The present study utilizes two types of seismic inversion, namely pre-stack and post-stack, to estimate subsurface petrophysical parameters, which are helpful in interpreting seismic sections. The relative performances of these two techniques are discussed in each steps of seismic inversion. The methods first applied to the composite trace near to well location and inverted for petrophysical parameters i.e. P- impedance, S- impedance, density, P-wave, S- wave velocity, V_P/V_S ratio, lambdarho and murho sections. The pre-stack inversion methods estimate these parameters directly from seismic data, while post-stack inversion methods estimate only P-impedance section. This P- impedance section is transformed into S- impedance, density, P- wave, S- wave, V_P/V_S ratio, lambdarho and murho sections using relationship derived from well log data. The analysis for composite trace shows that both inverted curves follow well log data nicely and depict good performance of the algorithm. The error analysis shows that the inverted curves from post-stack inversion have higher correlation and low RMS error, compared with the pre-stack inversion methods. Thereafter, the methods are applied to entire seismic section to estimate subsurface petrophysical parameters. The inverted sections from both the methods shows very high resolution image of the subsurface. The resolution of post-stack is slightly greater than pre-stack methods. The difference among these petrophysical parameters demonstrate that both methods produces similar results with small deviation particularly where larger values are present. These differences may also arise due to use of equations from well log data which is best appropriate for the traces which are very close to the well log data and shows deviation away from the boreholes. The interpretation of inverted results also indicates non-existence of any major reservoir.

ACKNOWLEDGEMENTS

One of the author (S.P. Maurya) is indebted to Science and Engineering Research Board, Department of Science

and Technology, New Delhi for financial supports in form of research project (Grant no PDF/2016/000888) under National Post-doctoral Fellowship scheme. Authors also acknowledge the CGG Veritas for providing seismic and well log data of Blackfoot field, Alberta, Canada.

Compliance with Ethical Standards

The authors declare that they have no conflict of interest and adhere to copyright norms.

REFERENCES

Berteussen, K. and Ursin, B., 1983. Approximate computation of the acoustic impedance from seismic data. Geophysics, 48(10), 1351-1358.

Campbell, D.C., Shimeld, J., Deptuck, M.E. and Mosher, D.C., 2015. Seismic stratigraphic framework and depositional history of a large upper Cretaceous and Cenozoic depocenter of southwest Nova Scotia Canada. Mar. Petrol. Geol., 65, 22-42.

Carrazzone, J.J., Chang, D., Lewis, C., Shah, P.M. and Wang, D.Y., 1996. Method for deriving reservoir lithology and fluid content from pre-stack inversion of seismic data. US Patent, 5, 583, 825.

Castagna, J.P., Batzle, M.L. and Eastwood, R.L., 1985. Relationships between compressional-wave and shear-wave velocities in clastic silicate rocks. Geophysics, 50(4), 571-581.

Chen, Q. and Sidney, S., 1997. Seismic attribute technology for reservoir forecasting and monitoring. The Leading Edge, 16(5), 445-448.

Clochard, V., Delépine, N., Labat, K. and Ricarte, P., 2009. Post-stack versus pre-stack stratigraphic inversion for CO_2 monitoring purposes: A case study for the saline aquifer of the Sleipner field. SEG Annual Meeting, Society of Exploration Geophysicists, pp. 2417-2421, https://doi.org/10.1190/1.3255345.

Cummings, D.I. and Arnott, R.W.C., 2005. Growth-faulted shelf-margin deltas: a new (but old) play type offshore Nova Scotia. B. Can. Petrol. Geol., 53(3), 211-236.

Downton, J.E., 2005. Seismic parameter estimation from AVO inversion. PhD Thesis, University of Calgary, Department of Geology and Geophysics.

Fatti, J.L., Smith, G.C., Vail, P.J., Strauss, P.J. and Levitt, P.R., 1994. Detection of gas in sandstone reservoirs using avo analysis: A 3-d seismic case history using the geo-stack technique. Geophysics, 59(9), 1362-1376.

Ferguson, R.J. and Margrave, G.F., 1996. A simple algorithm for band-limited impedance inversion. CREWES research report, 8(21), 1-10.

Gardner, G., Gardner, L. and Gregory, A., 1974. Formation velocity and density-the diagnostic basics for stratigraphic traps. Geophysics, 39(6), 770-780.

Gholami, A., 2016. A fast automatic multichannel blind seismic inversion for high-resolution impedance recovery. Geophysics, 81(5), V357-V364.

Goodway, B., 2001. AVO and Lamé constants for rock parameterization and fluid detection. CSEG Recorder, 26(6), 39-60.

Goodway, B., Chen, T. and Downton, J., 1997. Improved AVO Fluid detection and Lithology discrimination using Lamé petrophysical parameters; "λρ" $\mu\rho$ $\lambda\mu$ Fluid Stack" from P and S inversions. SEG Annual Meeting, Society of Exploration Geophysicists, pp.183-186.

Kidston, A.G., Brown, D.E., Smith, B.M. and Altheim, B., 2005. The Upper Jurassic Abenaki Formation, Offshore Nova Scotia: A Seismic and Geologic Perspective. Canada-Nova Scotia Offshore Petroleum Board, Halifax, Nova Scotia, p.168.

Kidston, A.G., Smith, B.M., Brown, D.E., Makrides, C. and Altheim, B., 2007. Nova Scotia Deepwater post-drill analysis 1982-2004. Unpublished Report to the Canada-Nova Scotia Offshore Petroleum Board, p.181.

Krebs, J.R., Anderson, J.E., Hinkley, D., Neelamani, R., Lee, S., Baumstein, A. and Lacasse, M.D., 2009. Fast full-wave field seismic inversion using encoded sources. Geophysics, 74(6), WCC177-WCC188.

Latimer, R.B., Davidson, R. and Van Riel, P., 2000. An interpreter's guide to understanding and working with seismic-derived acoustic impedance data. The leading edge, 19(3), 242-256.

Lindseth, R.O., 1979. Synthetic sonic logs-a process for stratigraphic interpretation. Geophysics, 44(1), 3-26.

Mallick, S., 1995. Model-based inversion of amplitude-variations-with-offset data using a genetic algorithm. Geophysics, 60(4), 939-954.

Matlab and Statistics Toolbox Release, 2015b. The Math Works Inc. Natick Massachusetts United States.

Maurya, S. and Singh, K.H., 2015, LP and ML sparse spike inversion for reservoir characterization- a case study from Blackfoot area Alberta Canada. 77th EAGE Conference and Exhibition, 1st – 4th June, Madrid, Spain.

Maurya, S.P. and Singh, K.H., 2017. Band limited impedance inversion of blackfoot field, Alberta, Canada. J. Geophysics, 38(1), 57-61.

Maurya, S.P., Singh, K.H. and Singh, N.P., 2018b. Qualitative and quantitative comparison of geostatistical techniques of porosity prediction from the seismic and logging data: a case study from the Blackfoot Field Alberta Canada. Mar. Geophys. Res., 1-21, https://doi.org/10.1007/s11001-018-9355-6

Maurya, S.P., Singh, K.H., Kumar, A. and Singh, N.P., 2018a. Reservoir characterization using Post-Stack seismic inversion techniques based on real coded genetic algorithm. J. Geophysics, 39(2), 95-103.

Moncayo, E., Tchegliakova, N. and Montes, L., 2012. Pre-stack seismic inversion based on a genetic algorithm: A case from the Llanos Basin (Colombia) in the absence of well information. CT and F-CienciaTecnologíay Futuro, 4(5), 5-20.

Morozov, I.B. and Ma, J., 2009. Accurate post-stack acoustic impedance inversion by well-log calibration. Geophysics, 74(5), R59-R67.

Pendrel, J., 2006. Seismic inversion - a critical tool in reservoir characterization. Scandinavian oil-gas magazine, 5(6), 19-22.

Russell, B., 1999. Comparison of post-stack seismic inversion methods. SEG Technical Program Expanded Abstracts, p.10.

Schuster, G.T., 2017. Seismic inversion. Society of Exploration Geophysicists. p1-353, https://doi.org/10.1190/1.9781560803423.

Shu-jin, Y., 2007. Progress of pre-stack inversion and application in exploration of the lithological reservoirs. Prog. in geophy., 3, p.032.

Smith, G. and Gidlow, P., 1987.Weighted stacking for rock property estimation and detection of gas. Geophys. Prospect., 35(9), 993-1014.

Srivastava, R. and Maultzsch, S., 2018. Integration of results from two seismic inversion methods – A Case Study. In 80th EAGE Conference and Exhibition, 11th-14th June, Copenhagen, Denmark.

Vardy, M.E., Clare, M.A., Vanneste, M., Forsberg, C.F. and Dix, J.K., 2018. Seismic inversion for site characterization: When, Where and Why Should We Use It? In Offshore Technology Conference, 30th April – 3rd May, NRG Park, Houston, Texas, USA, https://doi.org/10.4043/28730-MS.

Received on: 23.7.18; Revised on: 21.9.18; Accepted on: 28.9.18